

Quasicircular Orbital Parameters for Numerical Relativity Revisited

Alessandro Ciarfella,¹ James Healy,¹ Carlos O. Lousto,¹ and Hiroyuki Nakano²

¹*Center for Computational Relativity and Gravitation,
School of Mathematical Sciences, Rochester Institute of Technology,
85 Lomb Memorial Drive, Rochester, New York 14623, USA*
²*Faculty of Law, Ryukoku University, Kyoto 612-8577, Japan*

(Dated: June 18, 2024)

In the post-Newtonian (PN) expansion, we extend the determination of quasicircular orbital parameters to be used by subsequent full numerical simulations to the 3.5PN order, and find that this leads to lower eccentricities, e , than with our previous method that used up to 3PN order. We also supplement the computation of the radial infall due to radiation reaction and the location of the center of mass to 3.5PN order, providing explicit formulas. In addition, we consider the small mass ratio limit by explicitly including the Schwarzschild and Kerr limits, the later in quasi-isotropic as well as in our standard use of ADMTT coordinates. We evolve binaries with a $q = 1/16$ mass ratio by using 3PN, 3.5PN, 3.5PN+Schwarzschild, 3.5PN+KerrQISO and 3.5PN+KerrADMTT quasicircular data for three different configurations where the larger hole intrinsic spins are $\chi^z = -0.8, -0.4$ and $+0.8$. Using different measures of eccentricity from the black hole trajectories and from the waveform amplitudes and phases, we determine a systematic reduction of eccentricities with respect to the 3PN initial values by factors of up to an order of magnitude, and reaching the desired $e \sim 10^{-3}$ threshold.

PACS numbers: 04.25.dg, 04.25.Nx, 04.30.Db, 04.70.Bw

I. INTRODUCTION

The breakthroughs in numerical relativity (NR) [1–3] have enabled the detailed modeling of gravitational waves from the merger of binary black holes (BBHs), predictions eventually first detected ten years afterwards by LIGO [4]. Since then, improvements in the modeling of gravitational waves [5] and the creation of full numerical simulations catalogs [6–8] have gone along with the detection of over a hundred BBH mergers [9].

To represent the most likely configurations at the late inspiral stages of the binaries, quasicircular (QC) initial parameters have been chosen to create the first round of simulations to populate NR catalogs. Historically, two main approaches have been used in order to achieve the initial parameters leading to QC orbits. The first was the minimization of an effective potential [10] which lead to families of close binaries successfully evolved in the Lazarus approach [11], previous to the 2005 breakthroughs. It was then realized that the post-Newtonian (PN) approach lead to an alternative approximation to QC orbits [11]. Those studies were extended and formalized to third post-Newtonian (3PN) order in Ref. [12] and served to produce low eccentricity simulations that populated the RIT catalogs [7, 13–15] for comparable mass binaries, then used directly to obtain independently parameter estimations for the O1/O2 LIGO observations [16].

In this paper, we extend further this approach for the determination of QC parameters to the 3.5PN order to provide even lower eccentricities, $e \leq 10^{-3}$, suitable for modeling sources for the higher sensitivity third generation (3G) gravitational wave detectors and for the intermediate to small mass ratio binaries in the sensitivity

range of the LISA space detector. In fact, as we move from comparable mass ratios ($1/10 < q \leq 1$) to intermediate ones ($1/100 < q \leq 1/10$) [17], the computational requirements to perform simulations from a given initial orbital frequency (or binary's separation) increases as $\sim q^{-2}$, thus making it steeply costly. In practice, we will perform simulations from closer distances (thus decreasing computational costs to $\sim q^{-1}$) making it necessary to include higher PN orders in the QC orbit determinations, and possibly including the particle limit behavior in the Schwarzschild and Kerr backgrounds when $q \ll 1$.

These improved initial low eccentricity determinations also benefit the iterative approaches [18, 19] since they require evolutions of a couple of orbits for each iteration (becoming costly in the $q \ll 1$ regime), hence a lower initial e seed reduces the number of needed iterations to achieve a given level of $e \approx 0$.

II. APPROXIMATE INITIAL QUASICIRCULAR ORBITS

Here, we follow the procedure developed in Ref. [12] to obtain QC orbits, extending it to the full 3.5PN order, including all spin terms, in the Arnowitt-Deser-Misner transverse traceless (ADMTT) gauge that we found to reproduce well the initial coordinates chosen in our full numerical simulations. We will later proceed to supplement this approach by including the particle limit in the Schwarzschild and Kerr background cases, with applications to intermediate to small mass ratio BBH simulations.

A. 3.5PN Hamiltonian

From Ref. [20] the Hamiltonian at 3.5PN order in the ADMTT gauge can be written as

$$\begin{aligned} H = & H_N + H_{1\text{PN}} + H_{2\text{PN}} + H_{3\text{PN}} \\ & + H_{\text{LOSO}} + H_{\text{NLoso}} + H_{\text{NNLoso}} \\ & + H_{\text{LOS}_1 S_2} + H_{\text{NLOS}_1 S_2} \\ & + H_{\text{LOS}^2} + H_{\text{NLOS}^2} + H_{\text{LOS}^3}, \end{aligned} \quad (1)$$

where each Hamiltonian in the right-hand side of the above equation denotes Newtonian (N), 1PN, 2PN, 3PN, leading-order (LO) spin-orbit (SO), next-to-leading-order (NLO) SO, next-to-next-to-leading-order (NNLO) SO, LO $S_1 S_2$, NLO $S_1 S_2$, LO spin-squared (S^2), NLO S^2 , and LO cubic-in-spin (S^3) ones, respectively.

For the sake of simplicity, we will assume that the linear momenta of the black holes are opposed and directed along the y -axis and that the holes lie along the x -axis in our initial configuration, so that we can straightforwardly identify P_ϕ with L_z .

In absence of radiation reaction, the QC conditions in

polar coordinates read

$$P_r = 0, \quad \frac{\partial H}{\partial r} = 0. \quad (2)$$

These conditions give us an equation for $P_\phi = L_z$.

We then evaluate the orbital frequency, Ω , as

$$\Omega = \frac{\partial H}{\partial P_\phi}, \quad (3)$$

the tangential momentum, P_t , as

$$P_t = \frac{P_\phi}{r}, \quad (4)$$

and finally, the total ADM mass,

$$M_{\text{ADM}} = M + H, \quad (5)$$

where $M = m_1 + m_2$.

In the following, we will adopt the units $G = 1 = c$, and notation, $q = m_2/m_1 \leq 1$ for the mass ratio, with $\eta = q/(1+q)^2$, the intrinsic spins $\vec{\chi}_i = \vec{S}_i/m_i^2$, and r is the orbital distance between the two black holes.

The explicit results of evaluating the equations above, computed at 3.5PN order, in terms of Ω , are

$$\begin{aligned} P_t = & \frac{Mq}{(1+q^2)} \left\{ (M\Omega)^{1/3} + \frac{(15+29q+15q^2)(M\Omega)}{6(1+q)^2} - \frac{2((4+3q)\chi_{1z}+q(3+4q)\chi_{2z})(M\Omega)^{4/3}}{3(1+q)^2} \right. \\ & + \frac{1}{72(1+q)^4} [9(49-8\chi_{1x}^2+4\chi_{1y}^2+4\chi_{1z}^2) \\ & - 72q(-20+2\chi_{1x}^2-\chi_{1y}^2-\chi_{1z}^2+2\chi_{1x}\chi_{2x}-\chi_{1y}\chi_{2y}-\chi_{1z}\chi_{2z}) \\ & - 9q^4(-49+8\chi_{2x}^2-4\chi_{2y}^2-4\chi_{2z}^2) \\ & - 72q^3(-20+2\chi_{1x}\chi_{2x}+2\chi_{2x}^2-\chi_{1y}\chi_{2y}-\chi_{2y}^2-\chi_{1z}\chi_{2z}-\chi_{2z}^2) \\ & + q^2(1997-72\chi_{1x}^2+36\chi_{1y}^2+36\chi_{1z}^2-288\chi_{1x}\chi_{2x}-72\chi_{2x}^2+144\chi_{1y}\chi_{2y}+36\chi_{2y}^2 \\ & + 144\chi_{1z}\chi_{2z}+36\chi_{2z}^2)](M\Omega)^{5/3} \\ & - \frac{((16+29q+22q^2+7q^3)\chi_{1z}+q(7+22q+29q^2+16q^3)\chi_{2z})(M\Omega)^2}{2(1+q)^4} \\ & + \frac{1}{5184(1+q)^6} [-36(-2223+696\chi_{1x}^2-60\chi_{1y}^2+4\chi_{1z}^2) \\ & + 36q^4(7480+483\pi^2+318\chi_{1x}^2-372\chi_{1y}^2-324\chi_{1z}^2+636\chi_{1x}\chi_{2x}-330\chi_{2x}^2-2664\chi_{1y}\chi_{2y} \\ & - 1296\chi_{2y}^2-872\chi_{1z}\chi_{2z}-1504\chi_{2z}^2)-36q^6(-2223+696\chi_{2x}^2-60\chi_{2y}^2+4\chi_{2z}^2) \\ & + 9q(483\pi^2-4(-6721+1368\chi_{1x}^2+372\chi_{1y}^2+596\chi_{1z}^2+576\chi_{1y}\chi_{2y}+168\chi_{1z}\chi_{2z})) \\ & + 2q^3(13041\pi^2+2(53681+5940\chi_{1x}^2-11124\chi_{1y}^2-11124\chi_{1z}^2+11448\chi_{1x}\chi_{2x} \\ & + 5940\chi_{2x}^2-37584\chi_{1y}\chi_{2y}-11124\chi_{2y}^2-12672\chi_{1z}\chi_{2z}-11124\chi_{2z}^2)) \\ & + 36q^2(483\pi^2-2(-3740+165\chi_{1x}^2+648\chi_{1y}^2+752\chi_{1z}^2 \\ & - 318\chi_{1x}\chi_{2x}-159\chi_{2x}^2+1332\chi_{1y}\chi_{2y}+186\chi_{2y}^2+436\chi_{1z}\chi_{2z}+162\chi_{2z}^2)) \\ & + 9q^5(483\pi^2-4(-6721+1368\chi_{2x}^2+576\chi_{1y}\chi_{2y}+372\chi_{2y}^2+168\chi_{1z}\chi_{2z}+596\chi_{2z}^2))] (M\Omega)^{7/3} \\ & + \frac{1}{432(1+q)^6} [288(1+q)^2(2+3q)\chi_{1z}^3+288q(1+q)^2(7+8q)\chi_{1z}^2\chi_{2z} \\ & + \chi_{1z}(288(-37+2\chi_{1x}^2+2\chi_{1y}^2)-72q(355+2\chi_{1x}^2-28\chi_{1y}^2+26\chi_{1x}\chi_{2x}-40\chi_{1y}\chi_{2y}) \\ & - 3q^3(4951+432\chi_{1x}^2-288\chi_{1y}^2+2640\chi_{1x}\chi_{2x}+6528\chi_{2x}^2-3264\chi_{1y}\chi_{2y}-3696\chi_{2y}^2-5232\chi_{2z}^2) \\ & - 18q^4(475+168\chi_{1x}\chi_{2x}+1048\chi_{2x}^2-192\chi_{1y}\chi_{2y}-560\chi_{2y}^2-928\chi_{2z}^2) \\ & - 72q^5(39+84\chi_{2x}^2-42\chi_{2y}^2-82\chi_{2z}^2)+q^2(-24235-2016\chi_{1x}^2+2304\chi_{1y}^2) \end{aligned}$$

$$\begin{aligned}
& -6768\chi_{1x}\chi_{2x} - 6768\chi_{2x}^2 + 9216\chi_{1y}\chi_{2y} + 4032\chi_{2y}^2 + 4896\chi_{2z}^2)) \\
& + q\chi_{2z}(216(-13 + 8\chi_{1x}^2 - 4\chi_{1y}^2) + 18q(-475 + 248\chi_{1x}^2 - 160\chi_{1y}^2 - 312\chi_{1x}\chi_{2x} + 48\chi_{1y}\chi_{2y}) \\
& - 72q^4(355 + 134\chi_{1x}\chi_{2x} + 218\chi_{2x}^2 - 40\chi_{1y}\chi_{2y} - 82\chi_{2y}^2 - 82\chi_{2z}^2) \\
& - 288q^5(37 + 22\chi_{2x}^2 - 8\chi_{2y}^2 - 8\chi_{2z}^2) \\
& + 3q^2(-4951 + 1248\chi_{1x}^2 - 1056\chi_{1y}^2 - 6960\chi_{1x}\chi_{2x} - 1008\chi_{2x}^2 + 1536\chi_{1y}\chi_{2y} + 432\chi_{2y}^2 + 432\chi_{2z}^2) \\
& + q^3(-24235 + 1008\chi_{1x}^2 - 1152\chi_{1y}^2 - 24912\chi_{1x}\chi_{2x} - 12384\chi_{2x}^2 \\
& \quad + 6624\chi_{1y}\chi_{2y} + 4896\chi_{2y}^2 + 4896\chi_{2z}^2)))](M\Omega)^{8/3} \}, \tag{6}
\end{aligned}$$

for the QC tangential linear momentum P_t ,

$$\begin{aligned}
M_{\text{ADM}} = M + \frac{Mq}{1+q^2} \Big\{ & -\frac{(M\Omega)^{2/3}}{2} + \frac{(9 + 19q + 9q^2)(M\Omega)^{4/3}}{24(1+q)^2} - \frac{((4 + 3q)\chi_{1z} + q(3 + 4q)\chi_{2z})(M\Omega)^{5/3}}{3(1+q)^2} \\
& + \frac{1}{48(1+q)^4} (81 - 48\chi_{1x}^2 + 24\chi_{1y}^2 + 24\chi_{1z}^2 + q(267 - 96\chi_{1x}^2 + 48\chi_{1y}^2 + 48\chi_{1z}^2 - 96\chi_{1x}\chi_{2x} \\
& + 48\chi_{1y}\chi_{2y} + 48\chi_{1z}\chi_{2z}) + q^4(81 - 48\chi_{2x}^2 + 24\chi_{2y}^2 + 24\chi_{2z}^2) \\
& + q^2(373 - 48\chi_{1x}^2 + 24\chi_{1y}^2 + 24\chi_{1z}^2 - 192\chi_{1x}\chi_{2x} - 48\chi_{2x}^2 + 96\chi_{1y}\chi_{2y} + 24\chi_{2y}^2 \\
& + 96\chi_{1z}\chi_{2z} + 24\chi_{2z}^2) + q^3(267 - 96\chi_{1x}\chi_{2x} - 96\chi_{2x}^2 + 48\chi_{1y}\chi_{2y} + 48\chi_{2y}^2 + 48\chi_{1z}\chi_{2z} + 48\chi_{2z}^2))(M\Omega)^2 \\
& - \frac{((72 + 140q + 96q^2 + 27q^3)\chi_{1z} + q(27 + 96q + 140q^2 + 72q^3)\chi_{2z})(M\Omega)^{7/3}}{18(1+q)^4} \\
& - \frac{1}{10368(1+q)^6} [5(9(-1215 + 960\chi_{1x}^2 + 96\chi_{1y}^2 - 416\chi_{1z}^2) \\
& - 9q(401 + 246\pi^2 - 2112\chi_{1x}^2 - 1056\chi_{1y}^2 + 736\chi_{1z}^2 \\
& - 1152\chi_{1y}\chi_{2y} + 192\chi_{1z}\chi_{2z}) + 9q^6(-1215 + 960\chi_{2x}^2 + 96\chi_{2y}^2 - 416\chi_{2z}^2) \\
& - 9q^2(-9145 + 984\pi^2 - 816\chi_{1x}^2 - 2496\chi_{1y}^2 \\
& - 64\chi_{1z}^2 + 288\chi_{1x}\chi_{2x} + 528\chi_{2x}^2 - 4800\chi_{1y}\chi_{2y} - 672\chi_{2y}^2 + 832\chi_{1z}\chi_{2z} - 288\chi_{2z}^2) \\
& - 9q^4(-9145 + 984\pi^2 + 528\chi_{1x}^2 - 672\chi_{1y}^2 - 288\chi_{1z}^2 + 288\chi_{1x}\chi_{2x} \\
& - 816\chi_{2x}^2 - 4800\chi_{1y}\chi_{2y} - 2496\chi_{2y}^2 + 832\chi_{1z}\chi_{2z} \\
& - 64\chi_{2z}^2) - 9q^5(401 + 246\pi^2 - 2112\chi_{2x}^2 - 1152\chi_{1y}\chi_{2y} - 1056\chi_{2y}^2 + 192\chi_{1z}\chi_{2z} + 736\chi_{2z}^2) \\
& + q^3(149951 - 13284\pi^2 - 7776\chi_{1x}^2 + 19872\chi_{1y}^2 + 6048\chi_{1z}^2 - 5184\chi_{1x}\chi_{2x} \\
& - 7776\chi_{2x}^2 + 65664\chi_{1y}\chi_{2y} + 19872\chi_{2y}^2 - 11520\chi_{1z}\chi_{2z} + 6048\chi_{2z}^2)](M\Omega)^{8/3} \\
& + \frac{1}{24(1+q)^6} [24q(1+q)^2\chi_{1z}^3 + 24q(1+q)^2(1+2q)\chi_{1z}^2\chi_{2z} + q\chi_{2z}(9(-9 + 16\chi_{1x}^2 - 8\chi_{1y}^2) \\
& + 12q(-15 + 34\chi_{1x}^2 - 20\chi_{1y}^2 - 18\chi_{1x}\chi_{2x}) - 24q^4(31 + 17\chi_{1x}\chi_{2x} + 29\chi_{2x}^2 - 4\chi_{1y}\chi_{2y} - 10\chi_{2y}^2 - 10\chi_{2z}^2) \\
& - 12q^5(27 + 24\chi_{2x}^2 - 8\chi_{2y}^2 - 8\chi_{2z}^2) \\
& + 12q^2(-19 + 32\chi_{1x}^2 - 22\chi_{1y}^2 - 70\chi_{1x}\chi_{2x} - 10\chi_{2x}^2 + 8\chi_{1y}\chi_{2y} + 4\chi_{2y}^2 + 4\chi_{2z}^2) \\
& + 4q^3(-137 + 30\chi_{1x}^2 - 24\chi_{1y}^2 - 258\chi_{1x}\chi_{2x} - 132\chi_{2x}^2 + 48\chi_{1y}\chi_{2y} + 48\chi_{2y}^2 + 48\chi_{2z}^2)) \\
& + \chi_{1z}(-324 + 96\chi_{1x}^2 + 24q(-31 + 7\chi_{1x}^2 + \chi_{1y}^2 + \chi_{1x}\chi_{2x} + 4\chi_{1y}\chi_{2y}) - 3q^5(27 + 96\chi_{2x}^2 - 48\chi_{2y}^2 - 80\chi_{2z}^2) \\
& - 12q^4(15 + 6\chi_{1x}\chi_{2x} + 74\chi_{2x}^2 - 12\chi_{1y}\chi_{2y} - 40\chi_{2y}^2 - 56\chi_{2z}^2) \\
& - 12q^3(19 + 2\chi_{1x}^2 - 2\chi_{1y}^2 + 10\chi_{1x}\chi_{2x} + 76\chi_{2x}^2 - 32\chi_{1y}\chi_{2y} - 44\chi_{2y}^2 - 52\chi_{2z}^2) \\
& + 4q^2(-137 + 12\chi_{1x}^2 + 12\chi_{1y}^2 - 6\chi_{1x}\chi_{2x} - 78\chi_{2x}^2 \\
& + 84\chi_{1y}\chi_{2y} + 48\chi_{2y}^2 + 48\chi_{2z}^2))](M\Omega)^3 \}, \tag{7}
\end{aligned}$$

for the total ADM mass of the system, and

$$\begin{aligned}
\frac{r}{M} = \frac{1}{(M\Omega)^{2/3}} - \frac{3 + 5q + 3q^2}{3(1+q)^2} - \frac{((4 + 3q)\chi_{1z} + q(3 + 4q)\chi_{2z})(M\Omega)^{1/3}}{6(1+q)^2} \\
& + \frac{(M\Omega)^{2/3}}{72(1+q)^4} [18(-1 - 4\chi_{1x}^2 + 2\chi_{1y}^2 + 2\chi_{1z}^2) \\
& - 9q(-1 + 16\chi_{1x}^2 - 8\chi_{1y}^2 - 8\chi_{1z}^2 + 16\chi_{1x}\chi_{2x} - 8\chi_{1y}\chi_{2y} - 8\chi_{1z}\chi_{2z}) \\
& - 9q^3(-1 + 16\chi_{1x}\chi_{2x} + 16\chi_{2x}^2 - 8\chi_{1y}\chi_{2y} - 8\chi_{2y}^2 - 8\chi_{1z}\chi_{2z} - 8\chi_{2z}^2) - 18q^4(1 + 4\chi_{2x}^2 - 2\chi_{2y}^2 - 2\chi_{2z}^2) \\
& + q^2(62 - 72\chi_{1x}^2 + 36\chi_{1y}^2 + 36\chi_{1z}^2 - 288\chi_{1x}\chi_{2x} - 72\chi_{2x}^2 + 144\chi_{1y}\chi_{2y} + 36\chi_{2y}^2 + 144\chi_{1z}\chi_{2z} + 36\chi_{2z}^2)] \\
& + \frac{q((-26 - 6q + 3q^2)\chi_{1z} + (3 - 6q - 26q^2)\chi_{2z})(M\Omega)}{24(1+q)^4}
\end{aligned}$$

$$\begin{aligned}
& - \frac{(M\Omega)^{4/3}}{5184(1+q)^6} \left[-4509\pi^2 q - 27054\pi^2 q^3 - 4509\pi^2 q^5 + 144(9 + 12\chi_{1x}^2 + 66\chi_{1y}^2 - 14\chi_{1z}^2) \right. \\
& + 36q(1841 - 144\chi_{1x}^2 + 1128\chi_{1y}^2 + 8\chi_{1z}^2 - 432\chi_{1x}\chi_{2x} + 792\chi_{1y}\chi_{2y} + 240\chi_{1z}\chi_{2z}) \\
& + 144q^6(9 + 12\chi_{2x}^2 + 66\chi_{2y}^2 - 14\chi_{2z}^2) \\
& + 36q^5(1841 - 432\chi_{1x}\chi_{2x} - 144\chi_{2x}^2 + 792\chi_{1y}\chi_{2y} + 1128\chi_{2y}^2 + 240\chi_{1z}\chi_{2z} + 8\chi_{2z}^2) \\
& + 36q^2(7256 - 501\pi^2 - 858\chi_{1x}^2 + 1872\chi_{1y}^2 + 400\chi_{1z}^2 - 1428\chi_{1x}\chi_{2x} - 426\chi_{2x}^2 + 3024\chi_{1y}\chi_{2y} + 408\chi_{2y}^2 \\
& + 752\chi_{1z}\chi_{2z} + 216\chi_{2z}^2) + 36q^4(7256 - 501\pi^2 - 426\chi_{1x}^2 + 408\chi_{1y}^2 + 216\chi_{1z}^2 - 1428\chi_{1x}\chi_{2x} - 858\chi_{2x}^2 \\
& + 3024\chi_{1y}\chi_{2y} + 1872\chi_{2y}^2 + 752\chi_{1z}\chi_{2z} + 400\chi_{2z}^2) \\
& + 8q^3(49043 - 4914\chi_{1x}^2 + 6372\chi_{1y}^2 + 2484\chi_{1z}^2 - 8964\chi_{1x}\chi_{2x}) \\
& - 4914\chi_{2x}^2 + 20088\chi_{1y}\chi_{2y} + 6372\chi_{2y}^2 + 4608\chi_{1z}\chi_{2z} + 2484\chi_{2z}^2)] \\
& + \frac{(M\Omega)^{5/3}}{288(1+q)^6} \left[-36(1+q)^2(4+3q)\chi_{1z}^3 - 36q(1+q)^2(11+10q)\chi_{1z}^2\chi_{2z} + \chi_{1z}(144(3+2\chi_{1x}^2-\chi_{1y}^2) \right. \\
& + 12q(163+66\chi_{1x}^2-33\chi_{1y}^2+48\chi_{1x}\chi_{2x}-24\chi_{1y}\chi_{2y}) + q^2(3233+720\chi_{1x}^2-360\chi_{1y}^2+1584\chi_{1x}\chi_{2x} \\
& + 288\chi_{2x}^2-792\chi_{1y}\chi_{2y}-144\chi_{2y}^2-360\chi_{2z}^2) \\
& + 9q^4(147+48\chi_{1x}\chi_{2x}+80\chi_{2x}^2-24\chi_{1y}\chi_{2y}-40\chi_{2y}^2-128\chi_{2z}^2) \\
& + 18q^3(159+12\chi_{1x}^2-6\chi_{1y}^2+80\chi_{1x}\chi_{2x}+44\chi_{2x}^2-40\chi_{1y}\chi_{2y}-22\chi_{2y}^2-62\chi_{2z}^2) \\
& + 18q^5(15+12\chi_{2x}^2-6\chi_{2y}^2-22\chi_{2z}^2)) + q\chi_{2z}(54(5+4\chi_{1x}^2-2\chi_{1y}^2) \\
& + 9q(147+80\chi_{1x}^2-40\chi_{1y}^2+48\chi_{1x}\chi_{2x}-24\chi_{1y}\chi_{2y}) \\
& + q^3(3233+288\chi_{1x}^2-144\chi_{1y}^2+1584\chi_{1x}\chi_{2x}+720\chi_{2x}^2-792\chi_{1y}\chi_{2y}-360\chi_{2y}^2-360\chi_{2z}^2) \\
& + 12q^4(163+48\chi_{1x}\chi_{2x}+66\chi_{2x}^2-24\chi_{1y}\chi_{2y}-33\chi_{2y}^2-33\chi_{2z}^2) \\
& + 18q^2(159+44\chi_{1x}^2-22\chi_{1y}^2+80\chi_{1x}\chi_{2x}+12\chi_{2x}^2-40\chi_{1y}\chi_{2y}-6\chi_{2y}^2-6\chi_{2z}^2) \\
& \left. + 144q^5(3+2\chi_{2x}^2-\chi_{2y}^2-\chi_{2z}^2) \right], \tag{8}
\end{aligned}$$

for the ADMTT coordinate separation of the holes, r .

From these expressions, we can compute the relevant QC information of the BBH, given an initial orbital frequency. In what follows, we will use this information to compute the precise location of the individual holes with respect to the 3.5PN center of mass to optimize the initial numerical grids set up in the subsequent simulations, and also evaluate the instantaneous inwards momentum of the holes via radiation reaction, as in Ref. [12] it was observed to produce even smaller measured eccentricities in the actual full numerical simulations.

B. Center of mass vector

To conveniently specify locations of the two black holes, we need to compute the center of mass vector \vec{G} at 3.5PN order. The orbital components of the center of mass vector are derived in Ref. [21], the leading-order (LO) and next-to-leading order (NLO) spin-orbit (SO) part from Ref. [22], the S_1 - S_2 interaction term from Ref. [23], the S_1^2 (and S_2^2) part from Ref. [24] and finally the next-to-next-to-leading order (NNLO) SO component from Ref. [25]. Imposing $\vec{G} = 0$ as well as $x_1 - x_2 = r$, $y_1 = y_2$ and $z_1 = z_2$, we find

$$\begin{aligned}
x_1 = & \frac{qr}{1+q} + \frac{1}{16(1+q)^7} \left[8M(-1+q)q(1+q)^4 - \frac{8P^2(-1+q)(1+q)^8r}{M^2q} \right] \\
& + \frac{1}{16(1+q)^7} \left[\frac{4P^2(-1+q)(1+q)^6(5+8q+5q^2)}{Mq} \right. \\
& - \frac{4M^2(-1+q)q(1+q)^2(1+q^2)}{r} + \frac{2P^4(-1+q)(1+q)^{12}r}{M^4q^3} \left. \right] + \frac{P(-\chi_{1z}+q\chi_{2z})}{2(1+q)} \\
& + \frac{1}{16(1+q)^7} \left[\frac{2P^3(1+q)^8((2+q)\chi_{1z}-(1+2q)\chi_{2z})}{M^2q} + \frac{8MP(1+q)^4((5+3q)\chi_{1z}-q^2(3+5q)\chi_{2z})}{r} \right] \\
& + \frac{1}{16(1+q)^7} \left[\frac{P^5(1+q)^{10}(-(1+q(1+q)^2)\chi_{1z})+\chi_{2z}+q(2+q+q^2)\chi_{2z}}{M^4q^3} \right. \\
& + \frac{P^3(1+q)^6((-45-42q-2q^2+18q^3)\chi_{1z}+(-18+2q+42q^2+45q^3)\chi_{2z})}{Mqr} \\
& \left. + \frac{M^2P(1+q)^2}{r^2}((-79+q(-75+q(117+q(187+50q))))\chi_{1z} \right]
\end{aligned}$$

$$\begin{aligned}
& +q(-50+q(-187+q(-117+q(75+79q))))\chi_{2z})\Big] \\
& +\frac{1}{16(1+q)^7}\left[-\frac{9P^4(1+q)^{10}(-1+q^3)}{M^3q^3}+\frac{P^2(-1+q)(1+q)^4(-30-125q-198q^2-125q^3-30q^4)}{qr}\right. \\
& -\frac{P^6(-1+q)(1+q)^{14}(1+q^2)r}{M^6q^5}-\frac{1}{r^2}\left(2M^3q(1-12\chi_{1x}^2+10\chi_{1y}^2+10\chi_{1z}^2+q(2+26\chi_{1y}^2+26\chi_{1z}^2\right. \\
& \left.-4\chi_{1x}(7\chi_{1x}+2\chi_{2x})+4\chi_{1y}\chi_{2y}+4\chi_{1z}\chi_{2z}+q^4(-1+12\chi_{2x}^2-10\chi_{2y}^2-10\chi_{2z}^2)\right. \\
& \left.+q(5-20\chi_{1x}^2+22\chi_{1y}^2+22\chi_{1z}^2-8\chi_{1x}\chi_{2x}+4\chi_{2x}^2+4\chi_{1y}\chi_{2y}-6\chi_{2y}^2+4\chi_{1z}\chi_{2z}-6\chi_{2z}^2)\right. \\
& \left.-q^2(5+4\chi_{1x}^2-6\chi_{1y}^2-6\chi_{1z}^2-8\chi_{1x}\chi_{2x}-20\chi_{2x}^2\right. \\
& \left.+4\chi_{1y}\chi_{2y}+22\chi_{2y}^2+4\chi_{1z}\chi_{2z}+22\chi_{2z}^2)+q^3(4\chi_{2x}(2\chi_{1x}+7\chi_{2x})\right. \\
& \left.-2(1+2\chi_{1y}\chi_{2y}+13\chi_{2y}^2+2\chi_{1z}\chi_{2z}+13\chi_{2z}^2)))\Big)\Big], \tag{9}
\end{aligned}$$

$$y_1 = \frac{M^3q(\chi_{1x}(4\chi_{1y}+q\chi_{2y})-q\chi_{2x}(\chi_{1y}+4q\chi_{2y}))}{2(1+q)^4r^2}, \tag{10}$$

$$\begin{aligned}
z_1 = & \frac{P(\chi_{1x}-q\chi_{2x})}{2(1+q)}+\frac{1}{16M^4q^3(1+q)^5r^2}\left[-2M^2P^3q^2(1+q)^6r^2((2+q)\chi_{1x}-(1+2q)\chi_{2x})\right. \\
& \left.-4M^5Pq^3(1+q)^2r((6+q(9+5q))\chi_{1x}-q(5+9q+6q^2)\chi_{2x})\right] \\
& +\frac{1}{16M^4q^3(1+q)^5r^2}\left[P^5(1+q)^8r^2((1+q(1+q)^2)\chi_{1x}-(1+q(2+q+q^2))\chi_{2x})\right. \\
& \left.-M^3P^3q^2(1+q)^4r((-32+q(-50+q(-11+9q)))\chi_{1x}+(-9+q(11+50q+32q^2))\chi_{2x})\right. \\
& \left.+M^6Pq^3((47-3q(-17+q(19+q(33+10q))))\chi_{1x}+q(30+q(99+q(57-q(51+47q))))\chi_{2x})\right] \\
& +\frac{M^3q(\chi_{1x}(4\chi_{1z}+q\chi_{2z})-q\chi_{2x}(\chi_{1z}+4q\chi_{2z}))}{2(1+q)^4r^2}. \tag{11}
\end{aligned}$$

Note that here we use the variables $r = r(M\Omega)$ and $P = P_t(M\Omega) = P_1^y = -P_2^y$ in the previous subsection.

C. Radiation reaction

So far, all the parameters were calculated using the conservative part of the 3.5PN Hamiltonian. To take into account the radial momentum from the energy radiated by the binary, we also have to consider the energy flux and the mass rate change as follows.

$$\frac{dr}{dt} = -\left(\frac{dE_{\text{GW}}}{dt} + \dot{M}\right) \Big/ \left(\frac{dE_{\text{Orb}}}{dr}\right), \tag{12}$$

where the expressions for \dot{M} and E_{GW} for the non-precessing case are given in Ref. [26], while for those in the precessing case we can use Ref. [27].

Now, from the Hamilton equation

$$\dot{r} = \frac{\partial H}{\partial P_r}, \tag{13}$$

excluding higher P_r order terms, we derive the following relationship between \dot{r} and P_r ,

$$P_r = \dot{r} \left[\lim_{P_r \rightarrow 0} \frac{P_r}{\partial H / \partial P_r} \right]. \tag{14}$$

This leads to

$$\begin{aligned}
\frac{dr}{dt} = & \frac{M^{7/2}}{r^{7/2}} \left[\left(-\frac{13q^2}{4(q+1)^4} - \frac{3q}{2(q+1)^4} \right) \chi_{1y}\chi_{2x} + \left(-\frac{3q^3}{2(q+1)^4} - \frac{q^2}{4(q+1)^4} \right) \chi_{2y}\chi_{2x} \right. \\
& + \left(-\frac{q^2}{4(q+1)^4} - \frac{3q}{2(q+1)^4} \right) \chi_{1x}\chi_{1y} + \left(-\frac{3q^3}{2(q+1)^4} - \frac{13q^2}{4(q+1)^4} \right) \chi_{1x}\chi_{2y} \Big] \\
& + \frac{(1+q)^2 P_r}{qM} \left\{ 1 - \left(\frac{M}{r} \right) \frac{7q^2 + 15q + 7}{2(q+1)^2} + \left(\frac{M}{r} \right)^2 \frac{47q^4 + 229q^3 + 363q^2 + 229q + 47}{8(q+1)^4} \right. \\
& \left. + \left(\frac{M}{r} \right)^{5/2} \left[\left(\frac{q^2}{(q+1)^3} + \frac{11q}{4(q+1)^3} + \frac{3}{(q+1)^3} \right) \chi_{1z} + \left(\frac{3q^3}{(q+1)^3} + \frac{11q^2}{4(q+1)^3} + \frac{q}{(q+1)^3} \right) \chi_{2z} \right] \right\}
\end{aligned}$$

$$\begin{aligned}
& + \left(\frac{M}{r} \right)^3 \left[- \frac{121q^6}{16(q+1)^6} - \frac{\pi^2 q^5}{16(q+1)^6} - \frac{163q^5}{3(q+1)^6} - \frac{\pi^2 q^4}{4(q+1)^6} - \frac{1831q^4}{12(q+1)^6} - \frac{3\pi^2 q^3}{8(q+1)^6} \right. \\
& - \frac{3387q^3}{16(q+1)^6} - \frac{\pi^2 q^2}{4(q+1)^6} - \frac{1831q^2}{12(q+1)^6} - \frac{\pi^2 q}{16(q+1)^6} - \frac{163q}{3(q+1)^6} \\
& + \left(\frac{q^4}{2(q+1)^6} + \frac{11q^3}{2(q+1)^6} + \frac{14q^2}{(q+1)^6} + \frac{27q}{2(q+1)^6} + \frac{9}{2(q+1)^6} \right) \chi_{1x}^2 \\
& + \left(- \frac{9q^3}{4(q+1)^6} - \frac{27q^2}{4(q+1)^6} - \frac{27q}{4(q+1)^6} - \frac{9}{4(q+1)^6} \right) \chi_{1y}^2 \\
& + \left(- \frac{9q^3}{4(q+1)^6} - \frac{27q^2}{4(q+1)^6} - \frac{27q}{4(q+1)^6} - \frac{9}{4(q+1)^6} \right) \chi_{1z}^2 \\
& + \left(\frac{9q^6}{2(q+1)^6} + \frac{27q^5}{2(q+1)^6} + \frac{14q^4}{(q+1)^6} + \frac{11q^3}{2(q+1)^6} + \frac{q^2}{2(q+1)^6} \right) \chi_{2x}^2 \\
& + \left(- \frac{9q^6}{4(q+1)^6} - \frac{27q^5}{4(q+1)^6} - \frac{27q^4}{4(q+1)^6} - \frac{9q^3}{4(q+1)^6} \right) \chi_{2y}^2 \\
& + \left(- \frac{9q^6}{4(q+1)^6} - \frac{27q^5}{4(q+1)^6} - \frac{27q^4}{4(q+1)^6} - \frac{9q^3}{4(q+1)^6} \right) \chi_{2z}^2 \\
& + \left(\frac{3q^5}{(q+1)^6} + \frac{11q^4}{(q+1)^6} + \frac{16q^3}{(q+1)^6} + \frac{11q^2}{(q+1)^6} + \frac{3q}{(q+1)^6} \right) \chi_{1x}\chi_{2x} \\
& + \left(\frac{3q^5}{2(q+1)^6} + \frac{7q^4}{(q+1)^6} + \frac{11q^3}{(q+1)^6} + \frac{7q^2}{(q+1)^6} + \frac{3q}{2(q+1)^6} \right) \chi_{1y}\chi_{2y} \\
& + \left(\frac{3q^5}{2(q+1)^6} + \frac{7q^4}{(q+1)^6} + \frac{11q^3}{(q+1)^6} + \frac{7q^2}{(q+1)^6} + \frac{3q}{2(q+1)^6} \right) \chi_{1z}\chi_{2z} - \frac{121}{16(q+1)^6} \Big] \\
& + \left(\frac{M}{r} \right)^{7/2} \left[\left(- \frac{53q^5}{16(q+1)^6} - \frac{357q^4}{16(q+1)^6} - \frac{1097q^3}{16(q+1)^6} - \frac{743q^2}{8(q+1)^6} - \frac{421q}{8(q+1)^6} - \frac{9}{(q+1)^6} \right) \chi_{1z} \right. \\
& \left. + \left(- \frac{9q^6}{(q+1)^6} - \frac{421q^5}{8(q+1)^6} - \frac{743q^4}{8(q+1)^6} - \frac{1097q^3}{16(q+1)^6} - \frac{357q^2}{16(q+1)^6} - \frac{53q}{16(q+1)^6} \right) \chi_{2z} \right] \Big\}. \quad (15)
\end{aligned}$$

Finally, using Eq. (12), we can invert Eq. (15) and obtain P_r in terms of r . Given our particular initial configuration of the black holes along the x -axis, we have $P_r = P_{1x} = -P_{2x}$.

While this consistently completes our 3.5PN determination of the QC parameters for numerical simulations of BBHs, we would like to consider the special case of intermediate to small mass ratio binaries to extend and improve the reduction of eccentricity methods by considering for the large hole as a Schwarzschild or Kerr background (as a sort of resummation of PN terms) for the linear dependence with the mass ratio q , while preserving the 3.5PN terms at all higher powers of q .

D. Small mass ratio

In this subsection, we discuss an additional method, particularly useful to treat small mass ratio systems, in which we combine the particle limit and the 3.5PN treat-

ment of the problem. In particular, starting from the Kerr metric $g_{\mu\nu}^{\text{Kerr}}$ written in quasi-isotropic (QISO) coordinates, we have

$$\begin{aligned}
g_{\text{Kerr}}^{\mu\nu} p_\mu p_\nu &= E^2 g^{tt} + P_\phi^2 g^{\phi\phi} + 2g^{\phi t} EP_\phi \\
&= -1. \quad (16)
\end{aligned}$$

This expression gives us a formula to compute E which is our particle's Hamiltonian in QISO coordinates. To verify that this is the correct Hamiltonian, one can use the transformation of coordinates (see Ref. [28])

$$\begin{aligned}
x_{\text{QISO}}^k &= x_{\text{ADM}}^k + \xi^k \\
&= x_{\text{ADM}}^k - \frac{1}{4} \frac{M^2 a^2 n^k}{r_{\text{ADM}}} - \frac{7}{16} \frac{M^4 a^2 n^k}{r_{\text{ADM}}^3}, \quad (17)
\end{aligned}$$

where $a = S^z/M^2$ is the (nondimensional) spin of the more massive black hole, then perform an expansion of E obtained from Eq. (16) and verify that it reproduces the Hamiltonian in Eq. (1).

Using this method, the particle Hamiltonian in QISO coordinates (labeled simply by $r = r_{\text{QISO}}/M$ for the sake of simplicity) becomes

$$H_{\text{Kerr}} = - \frac{64r^3}{(a^2 - 4r^2 - 4r - 1)^3 + 16a^2 r^2 (a^2 - 4r(r+3) - 1)}$$

$$\begin{aligned}
& \times \left[-\frac{a^2(a-2r-1)(a+2r+1)\sqrt{\frac{4(L^2+4)}{a^2+4r^2-1} - \frac{4(a^2-1)(L^2+4)}{(a^2+4r^2-1)^2} + \frac{2a+2}{a^2+2ar+a} - \frac{2(a-1)}{a(a-2r-1)} + 1}}{4r} \right. \\
& + \frac{(a-2r-1)(a-2r+1)(a+2r-1)(a+2r+1)\sqrt{(2r+1)^2-a^2}}{64r^3} \\
& \times \frac{1}{(a^2+4r^2-1)^2} \left(-a^6 + a^4(3-4(r-3)r) + a^2(8r(r(-2L^2+2r(r+6)-7)-3)-3) \right. \\
& \left. \left. +(2r+1)^2(8r(r(2L^2+2r(r+2)+3)+1)+1) \right)^{1/2} - 2aL \right], \tag{18}
\end{aligned}$$

where $L = L^z/(M^2\eta)$ is the orbital angular momentum of the system. We point out that here, in the particle limit, we are assuming that the particle orbits in the equatorial plane.

Using the Hamiltonian in Eq. (18) and the method described in Sec. II A, one can derive the initial parameters in the particle limit $\eta \rightarrow 0$. The idea is now to combine the 3.5PN Hamiltonian with the particle limit Hamiltonian. To do so, we should first specify how a vector transforms under the coordinate transformation in Eq. (17),

$$\begin{aligned}
V_{\text{QISO}}^\mu(x_{\text{QISO}}^\sigma) &= V_{\text{ADM}}^\nu(x_{\text{ADM}}^\sigma) \frac{\partial x_{\text{ADM}}^\mu}{\partial x_{\text{QISO}}^\nu} \\
&= V_{\text{ADM}}^\nu(x_{\text{ADM}}^\sigma)(\delta_\nu^\mu + \xi_{,\nu}^\mu) \\
&= V_{\text{ADM}}^\mu(x_{\text{ADM}}^\sigma) + V_{\text{ADM}}^\nu(x_{\text{ADM}}^\sigma)\xi_{,\nu}^\mu, \tag{19}
\end{aligned}$$

relating the QISO coordinates to our preferred ADMTT gauge. We note that only the r -component of a vector will change under this coordinate transformation in Eq. (17).

For example, to compute the angular momentum P_ϕ , we have

$$P^\phi = P_{\text{3.5PN}}^\phi - P_{\text{3.5PN}}^\phi|_{\eta=0} + P_{\text{Kerr}}^\phi. \tag{20}$$

Similarly, we have

$$M^{\text{ADM}} = M_{\text{3.5PN}}^{\text{ADM}} - M_{\text{3.5PN}}^{\text{ADM}}|_{\eta=0} + M_{\text{Kerr}}^{\text{ADM}}, \tag{21}$$

and

$$r^{\text{QISO}} = r_{\text{3.5PN}}^{\text{QISO}} - r_{\text{3.5PN}}^{\text{QISO}}|_{\eta=0} + r_{\text{Kerr}}^{\text{QISO}}. \tag{22}$$

This distinction will be particularly important in the next section where we put to test this choice of the Kerr QISO coordinates to associate with the numerical coordinates versus the standard use of the ADMTT coordinates.

III. FULL NUMERICAL TECHNIQUES AND RESULTS

To test these theoretically improved choices of QC parameters, we perform a set of comparative full numerical

TABLE I. Number of orbits and time to merger

spin	id	ID	Name	orbits	t_{merg}
-0.8	0	3PN		6.57	1118
-0.8	1	3.5PN		6.93	1196
-0.8	2	3.5PN+Schwarzschild		7.04	1220
-0.8	3	3.5PN+KerrQISO		7.14	1241
-0.8	4	3.5PN+KerrADMTT		7.41	1302
-0.4	0	3PN		9.31	1476
-0.4	1	3.5PN		9.48	1513
-0.4	2	3.5PN+Schwarzschild		9.60	1538
-0.4	3	3.5PN+KerrQISO		9.66	1551
-0.4	4	3.5PN+KerrADMTT		9.72	1564
+0.8	0	3PN		22.74	2591
+0.8	1	3.5PN		22.09	2477
+0.8	2	3.5PN+Schwarzschild		22.31	2515
+0.8	3	3.5PN+KerrQISO		22.15	2488
+0.8	4	3.5PN+KerrADMTT		22.39	2528

simulations for configurations of current interest in the intermediated mass ratio regime. We will consider three basic configurations all bearing mass ratio $q = 1/16$ and spins of the larger black hole aligned or counteraligned with the orbital angular momentum of the system with intrinsic values $\chi = -0.8$, -0.4 , and $+0.8$, while the smaller hole is nonspinning. Initial separations of the binary have been chosen decreasingly, $d/M = 10.0$, 9.5 , and 8.0 , to compensate in part for the hangup/hangdown effect [29, 30] that prompts or delays merger for aligned or counteraligned spin-orbit coupling, respectively.

In Table I, we report the time to merger for each of the three spinning configurations while choosing five different methods to determine QC orbits. We identify the initial data by the methods as follows: id 0 is the 3PN order given in Ref. [12], id 1 is the improvement to 3.5PN order given here, id 2 is the partial resummation of the nonspinning terms into a Schwarzschild background for the linear in q terms, id 3 is the use of the Kerr metric in the QISO coordinates, and id 4 is the direct use of the ADMTT gauge transformation given in Eq. (17) to express also the Kerr metric in these ADMTT coordinates.

Notably, the results for the ‘hangdown’ configurations, with $\chi = -0.8$, and $\chi = -0.4$ show an increase in the merger times t_{merg} as well as in the number of orbits to merger with the additions of term in the QC method, i.e., with increasing id number. This can be interpreted

as due to a lowering of the eccentricity (as higher eccentricity is more efficient in radiating gravitational energy [31]), and will be confirmed below with direct measures of the eccentricity in each id case. The case $\chi = +0.8$ is less clear since the 3PN choice seems to produce eccentricity by an overshoot of the holes (at periastron instead of apastron), but it is also to note here the close starting point at a distance coordinate of $d/M = 8.0$ and the large number of orbits to merger due to the strong hangup effect.

We also display here the distance evolution and a measure of its eccentricity [32],

$$e \cos(\Omega t) \sim r^2 \ddot{r}, \quad (23)$$

for each of the three binary configurations studied here in Figs. 1–3. Each of those figures clearly show the different merger times in spite of starting at the same initial separation. The 3PN QC data is clearly the one displaying the largest eccentricity in coordinates. The amplitude of the orbital oscillations is more clearly exposed in the bottom plots of $r^2 \ddot{r}$ and show already a reduction factor of $\times 2\text{--}3$ for the 3.5PN choice, and further reduction for the resummation cases. Next we will quantify these eccentricities with invariant methods.

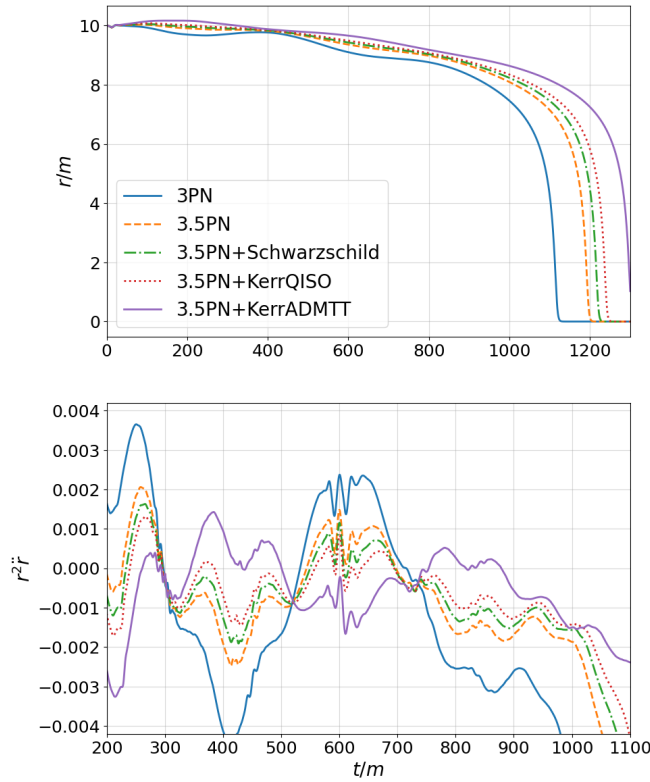


FIG. 1. Evolution of coordinate distance (top) and eccentricity measure $r^2 \ddot{r}$ (bottom) for the $q = 1/16, d = 10M, \chi = -0.8$ case.

To assess the eccentricity reduction more precisely in a coordinate independent way, we now consider the eccentricity measured by the amplitude and phase oscillation

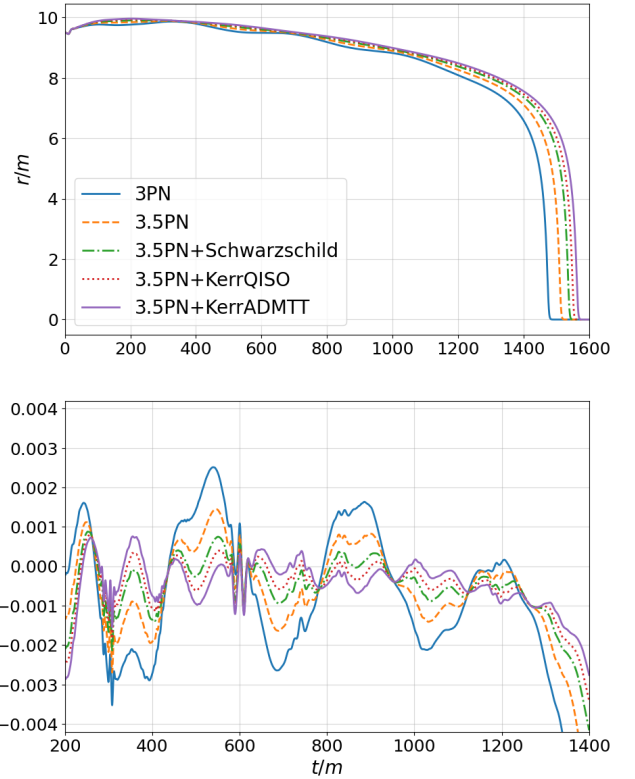


FIG. 2. Evolution of coordinate distance (top) and eccentricity measure $r^2 \ddot{r}$ (bottom) for the $q = 1/16, d = 9.5M, \chi = -0.4$ case.

of $\psi_{4(22)}$, the Weyl scalar waveform $(\ell, m) = (2, 2)$ mode as given in Ref. [12] given by

$$\psi_{4(22)} = A_{22}(t) \exp[i\varphi_{22}(t)]. \quad (24)$$

Hence we define the waveform-based eccentricity measures

$$e_{A22} = \left(\frac{8}{39} \right) \text{Amp} \left(\frac{A_{22}(t) - A_{22\text{sec}}(t)}{A_{22}(t)} \right), \quad (25)$$

$$e_{\omega 22} = \left(\frac{8}{21} \right) \text{Amp} \left(\frac{\omega_{22}(t) - \omega_{22\text{sec}}(t)}{\omega_{22}(t)} \right), \quad (26)$$

where $\omega_{22} = d\varphi_{22}/dt$.

The results of these evaluations of the eccentricity from the initial two orbits amplitude e_{A22} oscillations and frequency (when possible to measure meaningfully) $e_{\omega 22}$, are given in Table II, where we also included the e_{spd} obtained from the using the simple proper distance D along the line joining the horizons of the holes to evaluate $D^2 \dot{D}$ oscillations amplitude. While this different measures provide a possible definition of eccentricity (which is a Newtonian concept, not necessarily well nor uniquely defined in general relativity), we see the decreasing pattern with the successive approaches within each of the eccentricity definitions. For each of those measures, in

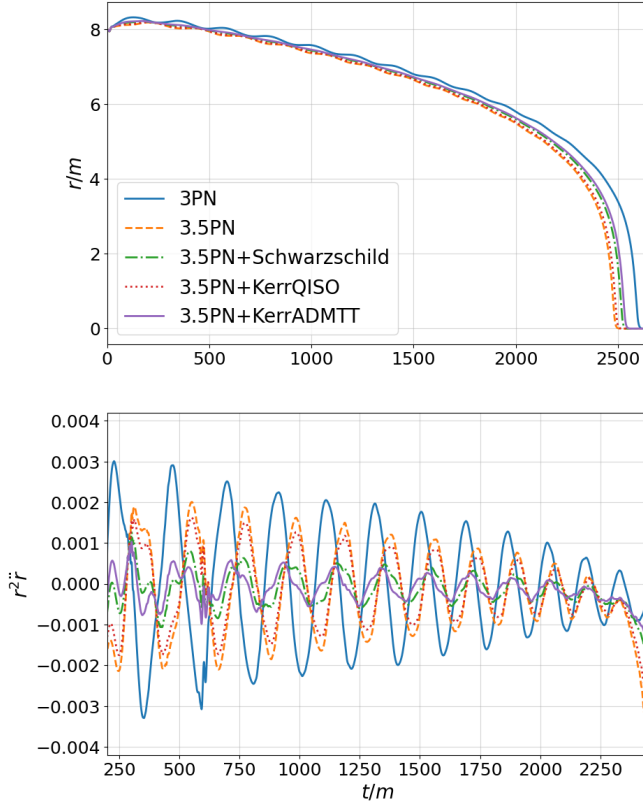


FIG. 3. Evolution of coordinate distance (top) and eccentricity measure $r^2\ddot{r}$ (bottom) for the $q = 1/16, d = 8M, \chi = +0.8$ case.

TABLE II. Waveforms eccentricity.

id	spin	e_{spd}	e_{A22}	$e_{\omega 22}$
0	-0.8	1.82e-2	3.04e-2	
1	-0.8	8.37e-3	1.03e-2	
2	-0.8	5.61e-3	7.37e-3	
3	-0.8	3.29e-3	4.53e-3	
4	-0.8	3.30e-3	1.90e-3	
0	-0.4	7.95e-3	7.09e-3	
1	-0.4	4.05e-3	3.52e-3	
2	-0.4	1.47e-3	1.18e-3	
3	-0.4	2.86e-4	1.46e-4	
4	-0.4	1.39e-3	1.48e-3	
0	+0.8	6.00e-3	5.72e-3	4.77e-3
1	+0.8	4.45e-3	4.27e-3	3.53e-3
2	+0.8	1.57e-3	1.49e-3	1.22e-3
3	+0.8	3.50e-3	3.36e-3	2.77e-3
4	+0.8	1.23e-3	1.18e-3	1.09e-3

particular for all e_{spd} , and e_{A22} , we see the same relative pattern behavior of decrease of eccentricity, favoring the Kerr background choice in ADMTT coordinates to be identified with the full numerical ones.

To quantify the magnitude of the differences due to eccentricity between the waveforms, we use the matching

TABLE III. Waveforms cross-matching.

	id2	0	1	2	3	4
spin -0.8	0	1.00000	0.71331	0.71980	0.71410	0.70901
	1	0.71331	1.00000	0.99664	0.95694	0.99937
	2	0.71980	0.99664	1.00000	0.97749	0.99311
	3	0.71410	0.95694	0.97749	1.00000	0.94604
	4	0.70901	0.99937	0.99311	0.94604	1.00000
	id2	0	1	2	3	4
spin -0.4	0	1.00000	0.97944	0.98241	0.97955	0.95987
	1	0.97944	1.00000	0.99988	1.00000	0.99671
	2	0.98241	0.99988	1.00000	0.99989	0.99536
	3	0.97955	1.00000	0.99989	1.00000	0.99667
	4	0.95987	0.99671	0.99536	0.99667	1.00000
	id2	0	1	2	3	4
spin +0.8	0	1.00000	0.99939	0.99976	0.99976	0.99925
	1	0.99939	1.00000	0.99978	0.99951	0.99902
	2	0.99976	0.99978	1.00000	0.99994	0.99939
	3	0.99976	0.99951	0.99994	1.00000	0.99940
	4	0.99925	0.99902	0.99939	0.99940	1.00000

measure,

$$\mathcal{M} \equiv \frac{\langle h_1 | h_2 \rangle}{\sqrt{\langle h_1 | h_1 \rangle \langle h_2 | h_2 \rangle}}, \quad (27)$$

as implemented via a complex overlap as described in Eq. (2) in Ref. [33]:

$$\langle h_1 | h_2 \rangle = 2 \int_{-\infty}^{\infty} \frac{df}{S_n(f)} [\tilde{h}_1(f) \tilde{h}_2(f)^*], \quad (28)$$

where $\tilde{h}(f)$ is the Fourier transform of $h(t)$ and $S_n(f)$ is the power spectral density of the detector noise (here, taken to be identically equal to 1 since we are interested in the direct waveforms comparisons). We adopt the leading modes $(\ell, m) = (2, 2)$ of ψ_4 for the computations and we do not maximize over an overall constant time shift and an overall constant phase shift as is usually done for parameter estimation of gravitational waves signals [34].

The results are presented in Table III as a cross-match between all the five approximation of QC parameters for the three cases of spins aligned and counteraligned studied here. We find the largest deviations between waveforms from the original 3PN data for the counteraligned spin configurations. We also note the preference of the ADMTT coordinates in the Kerr resummation case over the QISO coordinates identification with the numerical coordinates. The aligned spin case, with its tight orbits due to the strong hangup effect shows notable agreement between all waveforms.

In summary, all these results provide a consistent relative reduction of the eccentricity with the successive PN approximations to QC orbits and, notably, a preferences of the ADMTT gauge over the QISO in the Kerr case

(for Schwarzschild isotropic coordinates are also in the ADMTT gauge) for our full numerical set up.

We finally construct the strain h waveforms from the double integration of the Weyl scalar ψ_4 . The strain was computed by taking the Fourier transform of ψ_4 , removing modes in a small region around $\omega = 0$, then dividing by $-\omega^2$ and taking the inverse Fourier transform as detailed in Refs. [32, 35]. In Fig. 4, we display for all three spin cases the strain $(2, 2)$ -mode at an observer location $r = 113M$ for the QC choice of the 3.5PN+Kerr method in ADMTT coordinates. Note the smooth amplitude increase (after initial data settling) up to the merger characteristic of the non-eccentric (nonprecessing) black hole binaries. These prototypical waveforms will serve as a base for the construction of a first catalog of full numerical simulations in the intermediate mass ratio regime.

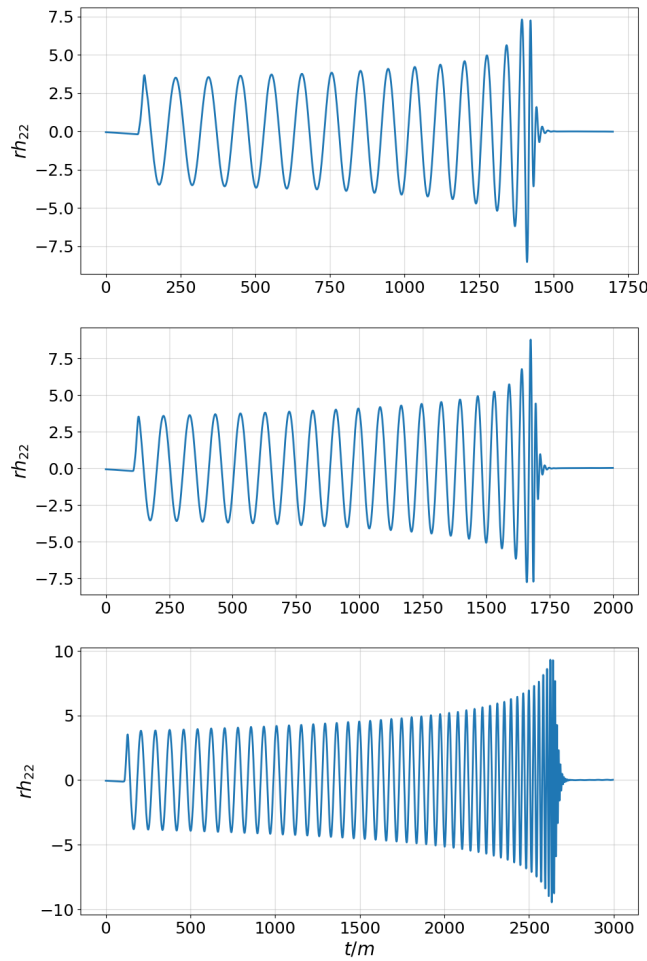


FIG. 4. Strain waveform for the 3.5PN+KerrADMTT QC data for the three cases studied here $q = 1/16$, $d = 10M$, $\chi = -0.8$ (top); $q = 1/16$, $d = 9.5M$, $\chi = -0.4$ (middle); $q = 1/16$, $d = 8M$, $\chi = +0.8$ (bottom); respectively.

IV. CONCLUSIONS AND DISCUSSION

We thus conclude through the analysis of different eccentricity measures that 3.5PN extension to QC parameters provides a clear benefit over 3PN for the close initial configurations needed when dealing with intermediate to small mass ratio binaries. We also have seen a further improvement when including the Schwarzschild limit and when spins are large the inclusion of the Kerr background in the ADMTT gauge expansion. These improvements on the low eccentricity initial parameters of intermediate to small mass ratio binaries will have a direct applications to the next generation of full numerical simulations catalogues to cover the parameter space relevant to ground third generation and space LISA gravitational wave observatories.

It is also worth noting here that the parameter space of the simulations should also include specific coverage of the initial eccentricity, in addition to the QC cases, since for some 3G and LISA sources it is expected that some residual eccentricity of the merging binary may survive while entering their sensitivity low frequency band. For instance, this can be achieved by choosing initial $e = 0.1$, 0.2 , etc. values from the inception of the full numerical simulations by using Ref. [36]. An especially intriguing case is GW190521, which matches well to highly eccentric comparable masses full numerical simulations [37].

ACKNOWLEDGMENTS

The authors thank Giuseppe Ficarra, and Yosef Zlochower for useful discussions. The authors also gratefully acknowledge the National Science Foundation (NSF) for financial support from Grant No. PHY-2207920. Computational resources were also provided by the Blue Sky, Green Prairies, and White Lagoon clusters at the CCRG-Rochester Institute of Technology, which were supported by NSF grants No. AST-1028087, No. PHY-1229173, No. PHY-1726215, and No. PHY-2018420. This work used the ACCESS allocation TG-PHY060027N, funded by NSF, and project PHY20007 Frontera, an NSF-funded Petascale computing system at the Texas Advanced Computing Center. HN is supported by Grants-in-Aid for Scientific Research, No. 21H01082, No. 21K03582 and No. 23K03432 from the Japan Society for the Promotion of Science (JSPS).

Appendix A: Approximate initial data in terms of radial distance

In many practical applications, one chooses to compare full numerical simulations from the same initial separation of the holes r . Here, we provide the explicit basic expressions for the initial QC parameters P_t and M_{ADM} , as well as the inverse to the Eq. (8) for $M\Omega(r)$.

The tangential linear momentum P_t expressed in term

of the separation of the holes r in ADMTT coordinates is given by

$$\begin{aligned} \frac{P_t}{M} = & \frac{1}{128} \sqrt{\frac{M}{r}} \left\{ 128 + \frac{256M}{r} - \frac{96((4+3q)\chi_{1z} + q(3+4q)\chi_{2z})}{(1+q)^2} \left(\frac{M}{r}\right)^{3/2} \right. \\ & + \frac{8}{(1+q)^2} \left[6(7-4\chi_{1x}^2 + 2\chi_{1y}^2 + 2\chi_{1z}^2) + q(41-48\chi_{1x}\chi_{2x} + 24\chi_{1y}\chi_{2y} + 24\chi_{1z}\chi_{2z} \right. \\ & \left. + 6q(7-4\chi_{2x}^2 + 2\chi_{2y}^2 + 2\chi_{2z}^2)) \right] \left(\frac{M}{r}\right)^2 \\ & - \frac{8((72+q(116+q(60+13q)))\chi_{1z} + q(13+4q(15+q(29+18q)))\chi_{2z})}{(1+q)^4} \left(\frac{M}{r}\right)^{5/2} \\ & + \frac{1}{(1+q)^4} \left[163\pi^2 q(1+q)^2 + 32(15-20\chi_{1x}^2 - 2\chi_{1y}^2 + 16\chi_{1z}^2) + 4q(-659+56\chi_{1z}^2 + 48\chi_{1x}\chi_{2x} \right. \\ & - 8\chi_{1y}(20\chi_{1y} + 27\chi_{2y}) - 8q^3(-15+20\chi_{2x}^2 + 2\chi_{2y}^2) + q^2(-659+48\chi_{1x}\chi_{2x} - 8\chi_{2y}(27\chi_{1y} + 20\chi_{2y})) \\ & + q(-1532+118\chi_{1x}^2 - 27\chi_{1z}^2 + 140\chi_{1x}\chi_{2x} + 118\chi_{2x}^2 - 16(8\chi_{1y}^2 + 29\chi_{1y}\chi_{2y} + 8\chi_{2y}^2)) \\ & \left. + 2(60+q(133+60q))\chi_{1z}\chi_{2z} + q(-27+8q(7+16q))\chi_{2z}^2) \right] \left(\frac{M}{r}\right)^3 \\ & + \frac{4}{(1+q)^6} \left[-20(1+q)^2(4+q)\chi_{1z}^3 - 60q(1+q)^2(3+2q)\chi_{1z}^2\chi_{2z} + \chi_{1z}(4(-87+80\chi_{1x}^2 - 20\chi_{1y}^2) \right. \\ & + 10q(-67-18\chi_{1y}^2 + 36\chi_{1x}(2\chi_{1x} + \chi_{2x})) + 12q^2(-21+40\chi_{1x}^2 + 70\chi_{1x}\chi_{2x} - 30\chi_{2x}^2 \\ & - 10(\chi_{1y}-2\chi_{2y})(\chi_{1y}+\chi_{2y}) + 10\chi_{2z}^2) + 5q^4(-29+24(\chi_{1x}-9\chi_{2x})\chi_{2x} \\ & + 24\chi_{2y}(\chi_{1y}+5\chi_{2y}) + 96\chi_{2z}^2) + q^5(-103-360\chi_{2x}^2 + 180\chi_{2y}^2 + 180\chi_{2z}^2) \\ & + q^3(27-20\chi_{1y}^2 + 40(2\chi_{1x}-3\chi_{2x})(\chi_{1x}+9\chi_{2x}) + 240\chi_{1y}\chi_{2y} + 660\chi_{2y}^2 + 420\chi_{2z}^2) \\ & + q\chi_{2z}(-103+360\chi_{1x}^2 - 180\chi_{1y}^2) + q(5(-29+216\chi_{1x}^2 - 120\chi_{1y}^2) \\ & - q(-27+252q+670q^2+348q^3-1080\chi_{1x}^2-360q\chi_{1x}^2+60(11+4q)\chi_{1y}^2) \\ & - 120(1+q)^2(1+3q)\chi_{1x}\chi_{2x} - 80q(1+q)^2(1+4q)\chi_{2x}^2 - 120(1+q)^2\chi_{1y}\chi_{2y} \\ & \left. + 20q(1+q)^2(1+4q)\chi_{2y}^2 + 20q(1+q)^2(1+4q)\chi_{2z}^2) \right] \left(\frac{M}{r}\right)^{7/2} \left. \right\}. \end{aligned} \quad (\text{A1})$$

The ADM mass of the system M_{ADM} expressed in term of the separation of the holes r in ADMTT coordinates is given by

$$\begin{aligned} M\Omega = & \frac{1}{384} \left(\frac{M}{r}\right)^{3/2} \left\{ 384 - \frac{192(3+5q+3q^2)M}{(1+q)^2 r} - \frac{96((4+3q)\chi_{1z} + q(3+4q)\chi_{2z})}{(1+q)^2} \left(\frac{M}{r}\right)^{3/2} \right. \\ & - \frac{24}{(1+q)^4} \left[16(1+q)^2(9+11q+9q^2) - 2(63+221q+319q^2+221q^3+63q^4) \right. \\ & \left. -(1+q)^2(6(7-4\chi_{1x}^2 + 2\chi_{1y}^2 + 2\chi_{1z}^2) \right. \\ & \left. + q(41-48\chi_{1x}\chi_{2x} + 24\chi_{1y}\chi_{2y} + 24\chi_{1z}\chi_{2z} + 6q(7-4\chi_{2x}^2 + 2\chi_{2y}^2 + 2\chi_{2z}^2))) \right] \left(\frac{M}{r}\right)^2 \\ & + \frac{72((16+30q+34q^2+13q^3)\chi_{1z} + q(13+34q+30q^2+16q^3)\chi_{2z})}{(1+q)^4} \left(\frac{M}{r}\right)^{5/2} \\ & + \frac{1}{(1+q)^6} \left[48(-10+38\chi_{1x}^2 - 43\chi_{1y}^2 - 7\chi_{1z}^2) + 4q^4(-10049+501\pi^2+930\chi_{1x}^2-660\chi_{1y}^2 \right. \\ & - 405\chi_{1z}^2 + 5124\chi_{1x}\chi_{2x} + 3546\chi_{2x}^2 - 4872\chi_{1y}\chi_{2y} - 3216\chi_{2y}^2 - 1914\chi_{1z}\chi_{2z} \\ & - 1233\chi_{2z}^2) + 4q^2(-10049+501\pi^2+3546\chi_{1x}^2-3216\chi_{1y}^2-1233\chi_{1z}^2+5124\chi_{1x}\chi_{2x} \\ & + 930\chi_{2x}^2 - 4872\chi_{1y}\chi_{2y} - 660\chi_{2y}^2 - 1914\chi_{1z}\chi_{2z} - 405\chi_{2z}^2) \\ & + 48q^6(-10+38\chi_{2x}^2 - 43\chi_{2y}^2 - 7\chi_{2z}^2) + q(501\pi^2+16(-686+498\chi_{1x}^2-513\chi_{1y}^2 \\ & - 135\chi_{1z}^2 + 360\chi_{1x}\chi_{2x} - 324\chi_{1y}\chi_{2y} - 144\chi_{1z}\chi_{2z})) \\ & + 6q^3(501\pi^2+4(-2470+490\chi_{1x}^2-390\chi_{1y}^2-197\chi_{1z}^2 \\ & + 1228\chi_{1x}\chi_{2x} + 490\chi_{2x}^2 - 1192\chi_{1y}\chi_{2y} - 390\chi_{2y}^2 - 446\chi_{1z}\chi_{2z} - 197\chi_{2z}^2)) \end{aligned}$$

$$\begin{aligned}
& +q^5(501\pi^2 + 16(-686 + 360\chi_{1x}\chi_{2x} \\
& + 498\chi_{2x}^2 - 324\chi_{1y}\chi_{2y} - 513\chi_{2y}^2 - 144\chi_{1z}\chi_{2z} - 135\chi_{2z}^2)) \Big] \left(\frac{M}{r}\right)^3 \\
& - \frac{12}{(1+q)^6} \left[12(1+q)^2(4+q)\chi_{1z}^3 + 36q(1+q)^2(3+2q)\chi_{1z}^2\chi_{2z} \right. \\
& + q\chi_{2z}(-27(-5+8\chi_{1x}^2-4\chi_{1y}^2) + q(385-648\chi_{1x}^2+360\chi_{1y}^2+72\chi_{1x}\chi_{2x}+72\chi_{1y}\chi_{2y}) \\
& + q^3(377-216\chi_{1x}^2+144\chi_{1y}^2+504\chi_{1x}\chi_{2x}+288\chi_{2x}^2+72\chi_{1y}\chi_{2y} \\
& - 72\chi_{2y}^2-72\chi_{2z}^2) + 9q^4(43+24\chi_{1x}\chi_{2x}+48\chi_{2x}^2-12\chi_{2y}^2-12\chi_{2z}^2) \\
& + 3q^2(121-216\chi_{1x}^2+132\chi_{1y}^2+120\chi_{1x}\chi_{2x} \\
& + 16\chi_{2x}^2+48\chi_{1y}\chi_{2y}-4\chi_{2y}^2-4\chi_{2z}^2) + 24q^5(7+8\chi_{2x}^2-2\chi_{2y}^2-2\chi_{2z}^2)) \\
& + \chi_{1z}(24(7-8\chi_{1x}^2+2\chi_{1y}^2)-9q(-43+48\chi_{1x}^2-12\chi_{1y}^2+24\chi_{1x}\chi_{2x}) \\
& + 27q^5(5+8\chi_{2x}^2-4\chi_{2y}^2-4\chi_{2z}^2) - q^2(-377+288\chi_{1x}^2-72\chi_{1y}^2+504\chi_{1x}\chi_{2x} \\
& - 216\chi_{2x}^2+72\chi_{1y}\chi_{2y}+144\chi_{2y}^2+72\chi_{2z}^2) - 3q^3(-121+16\chi_{1x}^2-4\chi_{1y}^2 \\
& \left. + 120\chi_{1x}\chi_{2x}-216\chi_{2x}^2+48\chi_{1y}\chi_{2y}+132\chi_{2y}^2+84\chi_{2z}^2) \right. \\
& \left. - q^4(-385+72\chi_{1x}\chi_{2x}-648\chi_{2x}^2+72\chi_{1y}\chi_{2y}+360\chi_{2y}^2+288\chi_{2z}^2)) \right] \left(\frac{M}{r}\right)^{7/2} \Big\}. \tag{A2}
\end{aligned}$$

The orbital angular frequency $M\Omega$ expressed in term of the separation of the holes r in ADMTT coordinates is given by

$$\begin{aligned}
\frac{M_{\text{ADM}}}{M} = & 1 + \frac{M}{384r} \left\{ -192 + \frac{48(7+q(13+7q))M}{(1+q)^2r} - \frac{96((4+3q)\chi_{1z}+q(3+4q)\chi_{2z})}{(1+q)^2} \left(\frac{M}{r}\right)^{3/2} \right. \\
& + \frac{24}{(1+q)^4} \left[9-8\chi_{1x}^2+4\chi_{1y}^2+4\chi_{1z}^2+q^4(9-8\chi_{2x}^2+4\chi_{2y}^2+4\chi_{2z}^2) \right. \\
& + 8q(2-2\chi_{1x}(\chi_{1x}+\chi_{2x})+\chi_{1y}(\chi_{1y}+\chi_{2y}) \\
& + \chi_{1z}(\chi_{1z}+\chi_{2z}))+8q^3(2-2\chi_{2x}(\chi_{1x}+\chi_{2x})+\chi_{2y}(\chi_{1y}+\chi_{2y})+\chi_{2z}(\chi_{1z}+\chi_{2z})) \\
& + q^2(13-8(\chi_{1x}^2+4\chi_{1x}\chi_{2x}+\chi_{2x}^2)+4(\chi_{1y}^2+4\chi_{1y}\chi_{2y}+\chi_{2y}^2) \\
& \left. + 4(\chi_{1z}^2+4\chi_{1z}\chi_{2z}+\chi_{2z}^2)) \right] \left(\frac{M}{r}\right)^2 \\
& - \frac{24((32+q(42+q(14+q)))\chi_{1z}+q(1+2q(7+q(21+16q)))\chi_{2z})}{(1+q)^4} \left(\frac{M}{r}\right)^{5/2} \\
& + \frac{1}{(1+q)^6} \left[537-1248\chi_{1x}^2+48\chi_{1y}^2+1200\chi_{1z}^2+q(-3497+243\pi^2(1+q)^4 \right. \\
& - 2784\chi_{1x}^2-144\chi_{1y}(5\chi_{1y}+8\chi_{2y})+144\chi_{1z}(23\chi_{1z}+10\chi_{2z}) \\
& + 3q^2(-9787+304\chi_{1x}^2+352\chi_{1z}^2+288\chi_{1x}\chi_{2x}+304\chi_{2x}^2 \\
& - 16(47\chi_{1y}^2+156\chi_{1y}\chi_{2y}+47\chi_{2y}^2)+2976\chi_{1z}\chi_{2z}+352\chi_{2z}^2) \\
& + 3q^5(179-416\chi_{2x}^2+16\chi_{2y}^2+400\chi_{2z}^2)-q^4(3497+2784\chi_{2x}^2+144\chi_{2y}(8\chi_{1y}+5\chi_{2y}) \\
& - 144\chi_{2z}(10\chi_{1z}+23\chi_{2z}))+q(-18707-1224\chi_{1x}^2+432\chi_{1x}\chi_{2x}+600\chi_{2x}^2 \\
& - 144(16\chi_{1y}^2+34\chi_{1y}\chi_{2y}+5\chi_{2y}^2)+72(43\chi_{1z}^2+82\chi_{1z}\chi_{2z}+\chi_{2z}^2)) \\
& + q^3(-18707+600\chi_{1x}^2+432\chi_{1x}\chi_{2x}-1224\chi_{2x}^2-144(5\chi_{1y}^2+34\chi_{1y}\chi_{2y}+16\chi_{2y}^2) \\
& \left. + 72(\chi_{1z}^2+82\chi_{1z}\chi_{2z}+43\chi_{2z}^2)) \right] \left(\frac{M}{r}\right)^3 \\
& - \frac{6}{(1+q)^6} \left[12(1+q)^2(12+5q)\chi_{1z}^3+12q(1+q)^2(29+22q)\chi_{1z}^2\chi_{2z} \right. \\
& + q\chi_{2z}(128-504\chi_{1x}^2+252\chi_{1y}^2+q(181-1536\chi_{1x}^2+24\chi_{1y}(35\chi_{1y}+9\chi_{2y}) \\
& + 4q^3(136+30\chi_{2x}(2\chi_{1x}+5\chi_{2x})+3(8\chi_{1y}-7\chi_{2y})\chi_{2y}-21\chi_{2z}^2) \\
& + 3q^2(27-176\chi_{1x}^2+112\chi_{1y}^2+160\chi_{1x}\chi_{2x}+112\chi_{2x}^2+136\chi_{1y}\chi_{2y}-8\chi_{2y}^2-8\chi_{2z}^2) \\
& + 24q^4(13+12\chi_{2x}^2-2\chi_{2y}^2-2\chi_{2z}^2)+4q(-22+6(-65\chi_{1x}^2+10\chi_{1x}\chi_{2x}+\chi_{2x}^2) \\
& + 3(77\chi_{1y}^2+44\chi_{1y}\chi_{2y}+\chi_{2y}^2)+3\chi_{2z}^2)) + \chi_{1z}(24(13-20\chi_{1x}^2+6\chi_{1y}^2) \\
& + q(544+348\chi_{1y}^2-24\chi_{1x}(47\chi_{1x}+26\chi_{2x})+96\chi_{1y}\chi_{2y}+4q^4(32+90\chi_{2x}^2-45\chi_{2y}^2-21\chi_{2z}^2) \\
& - 3q(-27+272\chi_{1x}^2-88\chi_{1y}^2+512\chi_{1x}\chi_{2x}-112\chi_{2x}^2-40\chi_{1y}\chi_{2y}+80\chi_{2y}^2+8\chi_{2z}^2) \\
& \left. - 4q^2(22+42\chi_{1x}^2-15\chi_{1y}^2+300\chi_{1x}\chi_{2x}-258\chi_{2x}^2+12\chi_{1y}\chi_{2y}+165\chi_{2y}^2+33\chi_{2z}^2) \right]
\end{aligned}$$

$$-q^3(-181 + 96(3\chi_{1x} - 11\chi_{2x})\chi_{2x} + 72\chi_{1y}\chi_{2y} + 600\chi_{2y}^2 + 192\chi_{2z}^2))) \left[\left(\frac{M}{r}\right)^{7/2} \right]. \quad (\text{A3})$$

-
- [1] F. Pretorius, Phys. Rev. Lett. **95**, 121101 (2005), gr-qc/0507014.
- [2] M. Campanelli, C. O. Lousto, P. Marronetti, and Y. Zlochower, Phys. Rev. Lett. **96**, 111101 (2006), gr-qc/0511048.
- [3] J. G. Baker, J. Centrella, D.-I. Choi, M. Koppitz, and J. van Meter, Phys. Rev. Lett. **96**, 111102 (2006), gr-qc/0511103.
- [4] B. P. Abbott *et al.* (LIGO Scientific, Virgo), Phys. Rev. Lett. **116**, 061102 (2016), arXiv:1602.03837 [gr-qc].
- [5] N. Afshordi *et al.* (LISA Consortium Waveform Working Group), (2023), arXiv:2311.01300 [gr-qc].
- [6] M. Boyle *et al.*, Class. Quant. Grav. **36**, 195006 (2019), arXiv:1904.04831 [gr-qc].
- [7] J. Healy and C. O. Lousto, Phys. Rev. D **105**, 124010 (2022), arXiv:2202.00018 [gr-qc].
- [8] D. Ferguson *et al.*, (2023), arXiv:2309.00262 [gr-qc].
- [9] R. Abbott *et al.* (KAGRA, VIRGO, LIGO Scientific), Phys. Rev. X **13**, 041039 (2023), arXiv:2111.03606 [gr-qc].
- [10] G. B. Cook, Phys. Rev. D **50**, 5025 (1994), arXiv:gr-qc/9404043.
- [11] J. G. Baker, M. Campanelli, C. Lousto, and R. Takahashi, Phys. Rev. **D65**, 124012 (2002), arXiv:astro-ph/0202469 [astro-ph].
- [12] J. Healy, C. O. Lousto, H. Nakano, and Y. Zlochower, Class. Quant. Grav. **34**, 145011 (2017), arXiv:1702.00872 [gr-qc].
- [13] J. Healy, C. O. Lousto, Y. Zlochower, and M. Campanelli, Class. Quant. Grav. **34**, 224001 (2017), arXiv:1703.03423 [gr-qc].
- [14] J. Healy, C. O. Lousto, J. Lange, R. O’Shaughnessy, Y. Zlochower, and M. Campanelli, Phys. Rev. **D100**, 024021 (2019), arXiv:1901.02553 [gr-qc].
- [15] J. Healy and C. O. Lousto, Phys. Rev. D **102**, 104018 (2020), arXiv:2007.07910 [gr-qc].
- [16] J. Healy, C. O. Lousto, J. Lange, and R. O’Shaughnessy, Phys. Rev. D **102**, 124053 (2020), arXiv:2010.00108 [gr-qc].
- [17] C. O. Lousto and J. Healy, Class. Quant. Grav. **40**, 09LT01 (2023), arXiv:2203.08831 [gr-qc].
- [18] H. P. Pfeiffer, D. A. Brown, L. E. Kidder, L. Lindblom, G. Lovelace, and M. A. Scheel, Class. Quant. Grav. **24**, S59 (2007), arXiv:gr-qc/0702106 [gr-qc].
- [19] A. Buonanno, L. E. Kidder, A. H. Mroue, H. P. Pfeiffer, and A. Taracchini, Phys. Rev. **D83**, 104034 (2011), arXiv:1012.1549 [gr-qc].
- [20] G. Schäfer and P. Jaranowski, Living Rev. Rel. **21**, 7 (2018), arXiv:1805.07240 [gr-qc].
- [21] T. Damour, P. Jaranowski, and G. Schaefer, Phys. Rev. **D62**, 021501 (2000), [Erratum: Phys. Rev. D63, 029903 (2000)], arXiv:gr-qc/0003051 [gr-qc].
- [22] T. Damour, P. Jaranowski, and G. Schafer, Phys. Rev. **D77**, 064032 (2008), arXiv:0711.1048 [gr-qc].
- [23] J. Steinhoff, G. Schafer, and S. Hergt, Phys. Rev. **D77**, 104018 (2008), arXiv:0805.3136 [gr-qc].
- [24] S. Hergt and G. Schaefer, Phys. Rev. **D78**, 124004 (2008), arXiv:0809.2208 [gr-qc].
- [25] J. Hartung and J. Steinhoff, Annalen Phys. **523**, 783 (2011), arXiv:1104.3079 [gr-qc].
- [26] P. Ajith, M. Boyle, D. A. Brown, S. Fairhurst, M. Hannam, I. Hinder, S. Husa, B. Krishnan, R. A. Mercer, F. Ohme, C. D. Ott, J. S. Read, L. Santamaria, and J. T. Whelan, (2007), arXiv:0709.0093 [gr-qc].
- [27] S. Ossokine, M. Boyle, L. E. Kidder, H. P. Pfeiffer, M. A. Scheel, and B. Szilagyi, Phys. Rev. **D92**, 104028 (2015), arXiv:1502.01747 [gr-qc].
- [28] S. Hergt and G. Schaefer, Phys. Rev. **D77**, 104001 (2008), arXiv:0712.1515 [gr-qc].
- [29] M. Campanelli, C. O. Lousto, and Y. Zlochower, Phys. Rev. **D74**, 041501(R) (2006), gr-qc/0604012.
- [30] J. Healy and C. O. Lousto, Phys. Rev. **D97**, 084002 (2018), arXiv:1801.08162 [gr-qc].
- [31] P. Peters, Phys. Rev. **136**, B1224 (1964).
- [32] M. Campanelli, C. O. Lousto, H. Nakano, and Y. Zlochower, Phys. Rev. **D79**, 084010 (2009), arXiv:0808.0713 [gr-qc].
- [33] H.-S. Cho, E. Ochsner, R. O’Shaughnessy, C. Kim, and C.-H. Lee, Phys. Rev. **D87**, 024004 (2013), arXiv:1209.4494 [gr-qc].
- [34] G. Lovelace *et al.*, Class. Quant. Grav. **33**, 244002 (2016), arXiv:1607.05377 [gr-qc].
- [35] C. Reisswig and D. Pollney, Class. Quant. Grav. **28**, 195015 (2011), arXiv:1006.1632 [gr-qc].
- [36] A. Ciarfella, J. Healy, C. O. Lousto, and H. Nakano, Phys. Rev. D **106**, 104035 (2022), arXiv:2206.13532 [gr-qc].
- [37] V. Gayathri, J. Healy, J. Lange, B. O’Brien, M. Szczepanczyk, I. Bartos, M. Campanelli, S. Klimenko, C. O. Lousto, and R. O’Shaughnessy, Nature Astron. **6**, 344 (2022), arXiv:2009.05461 [astro-ph.HE].